Sensor Selection With Composite Features in Identifying User-Intended Poses for Human-Prosthetic Interfaces

Tianshi Yu, *Graduate Student Member, IEEE*, Alireza Mohammadi, Ying Tan, *Fellow, IEEE*, Peter Choong, and Denny Oetomo, *Senior Member, IEEE*

Abstract— **A Human-Prosthetic Interface (HPI) serves to estimate and realise the limb pose intended by the human user, using the information obtained from sensors worn by the user. In recent studies, the HPI maps multi-joint limb poses (i.e. coordinated movement of the body and limbs) to the inputs of multiple sensors. This is in contrast to the conventional methods where each degree of freedom of the powered prosthesis is mapped to the input of one/a pair of sensors. In this approach, it is necessary to systematically select sensors that carry the most information for the intended set of poses, to improve system accuracy and/or minimise the number of sensors, thus the complexity, in the prosthetic system. In this paper, sensor selection process is systematically formulated to maximise the information contained in the input features for a given number of sensors. Most importantly, it accounts for *composite* features, which are features requiring information from multiple sensors. Such composite features exist and are important in HPIs as we seek to capture coordinated motion involving movements of multiple limb and body segments. A non-convex optimisation problem is formulated which accounts for the constraint introduced by the composite features. A projection matrix is utilised as the optimisation variable to select intended features for evaluation. The problem is solved by the proposed Sensor Selection with Composite Features (*SS-CF*) algorithm which adapts convex-relaxation techniques. The *SS-CF* is benchmarked against HPI with expert-selected sensors in the literature and against a greedy heuristic method. The outcome demonstrated the efficacy of the *SS-CF* algorithm.**

Index Terms— **Sensor selection, prosthetics, sparsity constraint optimisation.**

This work involved human subjects or animals in its research. Approval of all ethical and experimental procedures and protocols was granted by the University of Melbourne Human Research Ethics Committee under Project No. 11878.

Tianshi Yu, Alireza Mohammadi, Ying Tan, and Denny Oetomo are with the Department of Mechanical Engineering, University of Melbourne, Parkville, VIC 3010, Australia (e-mail: tianshiy@student.unimelb.edu.au; alireza.mohammadi@unimelb.edu.au; yingt@unimelb.edu.au; doetomo@unimelb.edu.au).

Peter Choong is with the Department of Surgery, St. Vincent's Hospital Melbourne, University of Melbourne, Fitzroy, VIC 3065, Australia (e-mail: pchoong@unimelb.edu.au).

Digital Object Identifier 10.1109/TNSRE.2023.3258225

I. Introduction

IN RECENT years, there has been great interest in developing Human-Prosthetic Interfaces (HPIs) that enable coordinated movement with the user's limb and body in order to produce human-like natural movements for people wearing upper limb prostheses [1], [2], [3], [4], [5], [6], [7], [8], [9], [10]. This differs from the more traditional approach in powered prostheses, where the movement of each degree of freedom is explicitly controlled by the human user through the signal from one/a pair of sensors (e.g. from the electromyography (EMG) signals of a pair of antagonistic muscles). One of the key challenges to coordinate such a movement is to identify the user-intended pose of the prosthesis based on the features that are the variables processed from wearable sensor signals forming the interface, such as inertia measurement units (IMUs) and surface EMG (sEMG).

Designing an appropriate HPI that can accurately reflect the user's intention is a challenging task due to the large variations of human users and the complexity of human movements. A natural solution is to use all available wearable sensors to provide as much information as can be obtained to the HPIs, as shown in [5]. On the other hand, using a low number of wearable sensors reduces the system complexity and is desired from the aspect of practical implementation [11]. It is imperative that the performance of the interface, in the form of the accuracy in the intention estimation, is maintained, else it would lead to ineffective operation, user frustration and device abandonment [12]. These two facts lead to the problem formulation in this paper: selecting the appropriate numbers of sensors from all available sensors, which provide the necessary information to identify the user-intended prosthetic pose from a set of target poses. This is known as the sensor selection problem in the literature [13], [14].

A common approach is to select the sensors based on evaluating the features with the most amount of discriminating information for detecting the user intention [11]. A feature that can be constructed out of the signal from a single sensor is termed a *direct* feature. The information contained in one sensor can be used to construct multiple features, hence one sensor can provide multiple direct features. There are also

features that require information from multiple sensors, which we shall define in this paper as *composite* features. The composite features have shown great benefits in designing HPIs, especially when coordinated motions are involved. For instance, the orientation of the forearm required the kinematic information of the upper arm, the trunk and the elbow joint. This means features such as wrist orientation are composite features, requiring information from multiple sensors (e.g. the IMUs) worn across the trunk, upper arm and forearm. These features are important in achieving coordinated movement of the prostheses and residual limb [2], [3], [15]. Other examples include muscle-synergy-related features, which require the sensor fusion of multiple sEMG electrodes on the residual limb and potentially the body of the user. Muscle synergy features could be more robust than commonly used time-domain sEMG features in prosthetic pose control [16]. Note that any dimension reduction technique such as Principal Component Analysis (PCA), e.g. in [15], creates a low-dimensional representation of the original features where each dimension is a composite feature.

To achieve coordinated movements, most studies select the features in their HPIs through the designer's experience, expertise and intuition, refined by a trial-and-error approach [3], [4], [5], [6], [7], [8], [9], [17], [18]. In recent years, there have been some studies to provide systematic methods for sensor selection (mostly sEMG), which have not considered composite features and are based on the performance of selected trained input-output models (e.g., classification and regression) [11], [13], [19], [20], [21]. In [13] and [19] the logistic regression model was used. The Sequential Forward Selection (SFS), which is a greedy heuristic method, was used in [11], [20], and [21]. In the SFS method, one sensor with all available features is added one at a time based on the classification performance until it reaches the required number of sensors. Nevertheless, the results did not take into account composite features which require certain combinations of sensors to be added together to be effective. In addition, these sensor selection algorithms are specific to the chosen machine learning model used for the intention estimation step, thus requiring time-consuming and repetitive training to be used for different models or to achieve a desired performance such as identification accuracy.

In this paper, we propose a systematic approach to select sensors with the most information to differentiate a given set of target poses achieved through coordinated motion, under the presence of composite features. For ease of presentation, we refer to the proposed algorithm as Sensor Selection with Composite Features (*SS-CF*), which is achieved by introducing a mapping matrix to characterise the relationship between the sensor and its direct/composite features, and to constrain the selected number of sensors/features. Such problem formulation leads to a non-convex optimisation problem for a given objective function to achieve as much separability as possible among the feature clusters of the target poses. Adapting existing optimisation techniques [22], [23] to solve the non-convex optimisation problem, the proposed *SS-CF* selects sensor combination for optimum performance for a given number of sensors. Furthermore, we adopt an objective function, which is based on the statistical property of the features [24], [25], [26], without repeating the input-output model training as in [11]. More specifically, the objective function is based on the class separability of the clusters representing each target pose, which maximises the intra-class variances of the features relative to their inter-class variances. While the proposed technique was designed to address sensor selection, it is also applicable to select features from the chosen sensors.

The effectiveness of the proposed algorithm is validated on the data collected in the context of prosthetic pose identification involving the coordinated movements of the upper limb and the trunk. The experiment was conducted in the transhumeral prostheses scenario with 10 subjects performing tasks involving 9 upper limb poses including three discrete prosthetic elbow poses that need to be differentiated. The proposed algorithm was implemented on the direct and composite features, including time-domain sEMG, muscle synergy and joint kinematics features. The features were obtained from the sensors attached to the residual limb (upper arm) and upper body of the subjects. The results of the proposed *SS-CF* method are compared to the existing sensor selection results in the literature and the SFS-type method.

II. SENSOR SELECTION WITH COMPOSITE FEATURES (SS-CF)

Sensor selection is a process to select a set of sensors from the available, which would yield the best performance. In our case, the performance is measured by having the highest information contained in the features. Each sensor provides sensor readings that contribute to one or more features.

This section formulates a class of sensor selection problems in the presence of composite features. It starts by defining sensor with composite features, followed by the definition of a matrix $\mathbf{A}'$ that characterises the relationship between the set of sensors and the set of features. With the help of $\mathbf{A}'$, the sensor selection is formulated as a finding the optimal subspace projection problem for a given objective function of the training data with constraints on the number of selected sensors and features. In general, such an optimisation problem is not convex, thus convexification techniques are discussed to provide feasible solutions to the formulated optimisation problem for sensor selection and/or feature selection.

Notation: We use lowercase letters for scalars, boldface lowercase letters for vectors, and boldface uppercase letters to denote matrices throughout this article. Let $\mathbb{R}$ and $\mathbb{R}^n$ denote the set of real numbers and an n-dimensional Euclidean space, respectively. Let $\mathbb{N}$ be the set of natural numbers. The key notations are listed in Table I.

A. Composite Features

A composite feature requires information from multiple sensors. A direct feature requires information from only one sensor. Assume that we have a collection of p sensors forming a sensor set $\mathcal{G} = \{g_1, g_2, \ldots, g_p\}$. Each sensor can contribute to one or more features. For the union of all available features, collected from these p sensors, we define the feature set $\mathcal{F} = \{f_1, f_2, \ldots, f_d\}$.

TABLE I
SUMMARY OF KEY NOTATIONS

Notation	Definition
$p \in \mathbb{N}$	Total number of sensors
$d \in \mathbb{N}$	Total dimension of features
$n \in \mathbb{N}$	Number of data samples
$q \in \mathbb{N}$	Number of selected sensors
$l \in \mathbb{N}$	Maximum number of selected features
$m \in \mathbb{N}$	Dimension after projection
$c \in \mathbb{N}$	Number of classes (target poses) to differentiate
$\alpha, \lambda \in \mathbb{R}$	Tuning parameter for the *SS-CF* algorithm
g_i	i^{th} sensor, $i \leq p$
f_i	i^{th} feature, $i \leq d$
$\mathbf{A}' \in \mathbb{R}^{d \times p}$	Sensor feature relationship matrix
$\mathbf{A} \in \mathbb{R}^{d \times p}$	Linear mapping constructed from $\mathbf{A}'$
$\mathbf{X} \in \mathbb{R}^{n \times d}$	Training data
$\mathbf{W} \in \mathbb{R}^{d \times m}$	Projection matrix with row sparsity
$\boldsymbol{\psi} \in \mathbb{R}^{p}$	Vector shows the selected sensors, based on $\mathbf{W}$ and $\mathbf{A}$
$\boldsymbol{\omega} \in \mathbb{R}^{d}$	Vector shows the selected features, based on $\mathbf{W}$
$\mathbf{S}_b \in \mathbb{R}^{d \times d}$	Inter-class scatter matrix
$\mathbf{S}_w \in \mathbb{R}^{d \times d}$	Intra-class scatter matrix
$\mathbf{y} \in \mathbb{R}^{n}$	Class label vector for each sample
$\mathbf{Y} \in \mathbb{R}^{n \times c}$	Dummy variable converted from $\mathbf{y}$
$\mathbf{B} \in \mathbb{R}^{c \times c}$	Short notation for $\frac{1}{n}\mathbf{Y}^T\mathbf{Y}$
$\boldsymbol{\Theta} \in \mathbb{R}^{c \times m}$	Scoring matrix
$\mathbf{1}_p \in \mathbb{R}^{p}$	All-ones column vector
$\text{diag}(\mathbf{v})$	Create a diagonal matrix with $\mathbf{v}$ as main diagonal
$tr(\mathbf{V})$	Trace of a square matrix $\mathbf{V}$
$\circ$	Hadamard product and power

TABLE II
EXAMPLE OF FEATURE AND SENSOR RELATIONSHIP

Feature	Sensor	
	g_1	g_2
f_1	1	0
f_2	1	1
f_3	0	1

The relationship between the features and the required sensors can be characterised by a matrix $\mathbf{A}' \in \mathbb{R}^{d \times p} = \left\{ a'_{ij} \right\}_{i=1,\dots,d,\ j=1,\dots,p}$ where

$$a'_{ij} = \begin{cases} 1 \ ; & \text{if feature } f_i \text{ needs information from } g_j \\ 0 \ ; & \text{else.} \end{cases} \quad (1)$$

Example 1: Assume that we have a feature set $\mathcal{F} = \{f_1, f_2, f_3\}$ extracted from two sensors g_1 and g_2. Table II describes the relationship between the feature set $\mathcal{F}$ and sensor set $\mathcal{G}$, where the entry filled with "1" means the measurements of the sensor contribute to the feature, and "0" otherwise.

From the table, we can see that feature f_1 is a direct feature because the information from g_1 is complete. The same for feature f_3. Whereas, feature f_2 is composite, since it requires the information from both sensor g_1 and g_2.

The matrix $\mathbf{A}'$ can be calculated using (1):

$$\mathbf{A}' = \begin{bmatrix} 1 & 0 \\ 1 & 1 \\ 0 & 1 \end{bmatrix}.$$

The resulting matrix $\mathbf{A}'$ reflects the feature-sensor arrangement as shown in Table II.   ∘

Remark 1: Note that there is no redundancy in sensor measurements, which means the same feature cannot be produced independently by another sensor.

The introduction of the matrix $\mathbf{A}'$ can also serve to determine when composite features are present. Specifically, a sensor set $\mathcal{G}$ contains composite features if $(\mathbf{A}')^T\mathbf{A}'$ has at least one non-zero off-diagonal term.

B. Problem Formulation

The sensor selection process includes choosing q sensors out of p sensors available for the analysis (where $p > q$), then evaluating through an optimisation process which combination of q sensors contain features that yield the most information in terms of identifying the user-intended poses. In this process, we also need to account for the constraint introduced by the presence of composite features.

The assessment is performed on a collected training data set $\mathbf{X} \in \mathbb{R}^{n \times d} = \left[\mathbf{x}_1, \mathbf{x}_2, \dots, \mathbf{x}_n \right]^T$, where the columns represent the d features and rows are the n samples. It should be noted that for the case of supervised training (which is the case in this paper), each row $\mathbf{x}_i^T$ ($i = 1, \dots, n$) is assigned a label, contained in a vector $\mathbf{y} \in \mathbb{R}^n$, corresponding to the associated target poses. There are c possible labels contained in a set $\mathcal{P} = \{1, 2, \dots, c\}$. In the problem in this paper, the labels represent the target poses to be achieved by the human user and the prosthesis.

This subsection will therefore present (i) a method to specify which features (from the q sensors) are to be evaluated by the use of a projection matrix, (ii) the formulation of the optimisation problem to find the optimal set of q sensors with respecting constraint introduced by composite features, and finally (iii) the objective function to be optimised in the context of this paper, which is the ability to accurately identify the target poses as intended by the human users. These are presented in the three respective subsections below.

1) Specifying Which Sensors or Features to Evaluate Using Projection Matrix W: In this work, we use a projection matrix $\mathbf{W}$ to specify which features are included when evaluating the performance as required by the objective function. The projection matrix has a specific structure of having some rows set to all zeros [24]. Multiplying the projection matrix with the training data $\mathbf{X}$ produces a resulting data representation containing only the effect of features multiplied with rows of $\mathbf{W}$ that are not set to all zeros.

Let $\mathbf{W} = \left[\mathbf{w}_1, \mathbf{w}_2, \dots, \mathbf{w}_m \right] \in \mathbb{R}^{d \times m}$ be the projection matrix and $\mathbf{Z}$ the result of the projection that satisfies $\mathbf{Z} = \mathbf{X}\mathbf{W} \in \mathbb{R}^{n \times m}$, where m is the number of dimensions after the projection and is less than or equal to the number of all available features d. If i^{th} row of $\mathbf{W}$ are all zeros, i.e. the squared sum of the elements is zero, the influence of the ith column of $\mathbf{X}$ in $\mathbf{Z}$ is zero. In other words, the contribution of feature f_i to $\mathbf{Z}$ is ignored. Note that multiple rows in $\mathbf{W}$ can be made all zeros. Removing selected features means that only the remainders are included in further consideration, such as in the evaluation of the information content. To exclude a sensor from the selected set, rows corresponding to features from the said sensor need to be assigned all zeros. This includes any composite features that require data from the said sensor. For instance, using the same setting as Example 1, if the 2nd and 3rd row of $\mathbf{W}$ are all zeros, the sensor g_2 will be excluded from the selected set.

This structure is referred to as row sparsity and can be indicated by a vector $\boldsymbol{\omega} = [\omega_1, \omega_2, \ldots, \omega_d]^T \in \mathbb{R}^d$, where the importance of feature f_i are proportional to the ω_i and the f_i are selected if i satisfy $\omega_i \neq 0$, and vice versa. The $\boldsymbol{\omega}$ gives the form

$$\boldsymbol{\omega} = (\mathbf{W} \circ \mathbf{W})\mathbf{1}_m, \tag{2}$$

where $\mathbf{1}_m = [1, 1, \ldots, 1]^T \in \mathbb{R}^m$, and the $\circ$ denotes the Hadamard (element-wise) product and power [27] of two matrices $\mathbf{V}, \mathbf{U} \in \mathbb{R}^{d \times m}$ defined as

$$\mathbf{H} = (\mathbf{V} \circ \mathbf{U})^{\circ \frac{1}{2}} = \{h_{ij}\}_{i=1,\ldots,d, \ j=1,\ldots,m}, \\ h_{ij} = (v_{ij}u_{ij})^{\frac{1}{2}}. \tag{3}$$

In this paper, the projection matrix $\mathbf{W}$ is not manually assigned for performance evaluation. Instead, $\mathbf{W}$ is obtained by solving the optimisation problem below.

2) General Formulation: Subsequently, we propose a general problem formulation for sensor selection accounting for the presence of composite features, which is a constrained optimisation problem to obtain the $\mathbf{W}$. The key problem is to obtain the required sensors based on the knowledge of selected (composite) features. Here, we utilise a linear mapping $\mathbf{A}$ constructed from $\mathbf{A}'$ in (1) to obtain a vector $\boldsymbol{\psi} = [\psi_1, \psi_2, \ldots, \psi_p]^T \in \mathbb{R}^p$ indicating the required sensors g_i where i satisfy $\psi_i \neq 0$. The $\boldsymbol{\psi}$ takes the form

$$\boldsymbol{\psi} = \mathbf{A}^T\boldsymbol{\omega}, \\ \mathbf{A} = \text{diag}(\mathbf{A}'\mathbf{1}_p)\mathbf{A}', \tag{4}$$

where $\text{diag}(\mathbf{v})$ creates a square diagonal matrix with vector $\mathbf{v}$ as the main diagonal, and the ith diagonal term of $\text{diag}(\mathbf{A}'\mathbf{1}_p)$ represents the maximum number of features can be obtained by selecting sensor g_i.

For any chosen objective/cost function and training data $\mathbf{X}$, a general form of such the intended optimisation is:

$$\max_{\mathbf{W}} / \min_{\mathbf{W}} J(\mathbf{X}, \mathbf{y}, \mathbf{W}), \tag{5}$$

$$\text{s.t. } \boldsymbol{\omega} = (\mathbf{W} \circ \mathbf{W})\mathbf{1}_m, \ \|\boldsymbol{\omega}\|_0 \leq l, \tag{6}$$

$$\boldsymbol{\psi} = \mathbf{A}^T\boldsymbol{\omega}, \ \|\boldsymbol{\psi}\|_0 = q, \tag{7}$$

where $\mathbf{y}$ contains the corresponding labels for the training data, which can be neglected if an unsupervised scenario is considered, $\|\cdot\|_p$ is the l_p-(pseudo)norm of the vector and when $p = 0$ it counts the non-zero entries of the vector. Equation (6), originated from (2), constrains the selected number of features by an upper bound of l. The selected features as reflected in $\boldsymbol{\omega}$ will require the set of sensors $\boldsymbol{\psi}$ reflected in (7), which captures the feature-sensor mapping through matrix $\mathbf{A}$. Finally, (7) also limits the number of sensors (the number of non-zero elements in $\boldsymbol{\psi}$) to q.

3) The Objective Function to Optimise: Next, an explicit objective function is required in place of (5) that is contextual to this application. For the HPI in this study, the key requirement in the process of sensor (and/or feature) selection is to successfully differentiate the user-intended prosthetic poses. As a result, an objective function was selected to maximise the "class separability" that evaluates how well

the clusters of the required target poses (i.e. classes) can be separated from one another relative to their individual spread in the feature space [28], [29]. In other words, the objective is to maximise the inter-class variance and minimise the intra-class variance. The two types of variances are evaluated by the inter-class and intra-class scatter matrix $\mathbf{S}_b \in \mathbb{R}^{d \times d}$ and $\mathbf{S}_w \in \mathbb{R}^{d \times d}$ given by

$$\mathbf{S}_b = \sum_{j=1}^{c} n_j(\mathbf{m}_j - \mathbf{m})(\mathbf{m}_j - \mathbf{m})^T, \tag{8}$$

$$\mathbf{S}_w = \sum_{j=1}^{c}\sum_{k=1}^{n_j} (\mathbf{x}_{j,k} - \mathbf{m}_j)(\mathbf{x}_{j,k} - \mathbf{m}_j)^T, \tag{9}$$

where $\mathbf{x}_{j,k}$ ($j = 1, \ldots, c, \ k = 1, \ldots, n_j$) represents the kth samples of the jth class by relabelling each observation $\mathbf{x}_i$ according to $\mathbf{y}$, n_j is the number of samples in the jth class, i.e., $\sum_{j=1}^{c} n_j = n$, and $\mathbf{m}_j \in \mathbb{R}^d$ is the mean of the jth class, computed from the sampled data in the jth class while $\mathbf{m} \in \mathbb{R}^d$ is the mean of all samples.

In order to formulate a scalar "class separability" measure, we adopt the ratio trace of the scatter matrices [24], [30]. A higher value of the scalar measure indicates a greater chance of achieving higher accuracy in identifying the target poses, as demonstrated in our previous work [28]. Substituting this scalar measure as the objective function in (5), the selection of sensors and features can be formulated as the following optimisation problem in the presence of composite features (see Section II-A):

$$\max_{\mathbf{W}} \ tr\left[(\mathbf{W}^T\mathbf{S}_w\mathbf{W})^{-1}(\mathbf{W}^T\mathbf{S}_b\mathbf{W})\right] \tag{10}$$

$$\text{s.t. } \boldsymbol{\omega} = (\mathbf{W} \circ \mathbf{W})\mathbf{1}_m, \ \|\boldsymbol{\omega}\|_0 \leq l \\ \boldsymbol{\psi} = \mathbf{A}^T\boldsymbol{\omega}, \ \|\boldsymbol{\psi}\|_0 = q, \tag{11}$$

where $tr(\mathbf{V})$ denotes the trace of any $m \times m$ square matrix which is defined as $tr(\mathbf{V}) = \sum_{i=1}^{m} v_{ii}$.

C. Convex Relaxation

The objective function (10) is non-convex with two non-convex constraints (11). Such optimisation problems are challenging to solve as many local minima exist [24], [25]. In order to make such problems tractable and solved efficiently, many techniques have been proposed to relax the problems by their convex approximates [22], [31].

In this paper, the non-convex objective function (10) is approximated by a least-square convex regression problem by adding a new optimisation variable called scoring matrix [23]. The constraints are reformulated as penalty functions [31]. The optimal projection and scoring matrix are obtained by fixing one and solving another [22] using gradient-based technique as described in [32].

When the convex-relaxation techniques are not applicable for some objective/cost, the greedy heuristic algorithms such as sequential forward selection (SFS) were proposed to find a feasible solution to the problem (10) with constraints (11). Although such algorithm is applicable to our problem formulation, given the existence of composite features we

doubt the solution by the heuristics is very likely to be suboptimal.

1) Objective Function Relaxation: The non-convex objective function in (10) is cast into a convex one. To do so, the class label $\mathbf{y}$ is turned into continuous variables using the dummy variables and scoring matrix [23]. Let $\mathbf{Y} = \left\{ y_{i,j} \right\}_{i=1,\ldots,n, j=1,\ldots,c} \in \mathbb{R}^{n \times c}$ denote the dummy variable of the label vector $\mathbf{y}$ where its elements are defined as

$$y_{ij} = \begin{cases} 1 & \text{if the } i^{\text{th}} \text{ observation belongs to } j^{\text{th}} \text{ class} \\ 0 & \text{else.} \end{cases}$$
(12)

The scoring matrix $\mathbf{\Theta}$ is defined as $\mathbf{\Theta} = \left[\boldsymbol{\theta}_1, \boldsymbol{\theta}_2, \ldots, \boldsymbol{\theta}_m \right] \in \mathbb{R}^{c \times m}$. Let matrix $\mathbf{B}$ be defined as $\mathbf{B} = \frac{1}{n} \mathbf{Y}^T \mathbf{Y}$. Instead of solving the non-convex objective (10), we can solve the following problem with a convex objective

$$\min_{\mathbf{W}, \mathbf{\Theta}} \frac{1}{2n} || \mathbf{Y}\mathbf{\Theta} - \mathbf{X}\mathbf{W} ||_F^2$$
(13)

$$\text{s.t. } \boldsymbol{\omega} = (\mathbf{W} \circ \mathbf{W})\mathbf{1}_m, \ \|\boldsymbol{\omega}\|_0 \le l$$

$$\boldsymbol{\psi} = \mathbf{A}^T \boldsymbol{\omega}, \ \|\boldsymbol{\psi}\|_0 = q$$
(14)

$$\mathbf{\Theta}^T \mathbf{B} \mathbf{\Theta} = \mathbf{I}_{m \times m},$$

where $\|\cdot\|_F$ denotes the Frobenius norm of a matrix defined as $\|\mathbf{V}\|_F = \sqrt{tr\left(\mathbf{V}^T \mathbf{V}\right)}$.

2) Constraints Relaxation: To relax the non-convex constraints on the number of sensors and features, the problem (13, 14) are solved sequentially for each vector pair $\mathbf{w}_k$ in $\mathbf{W}$ and $\boldsymbol{\theta}_k$ in $\mathbf{\Theta}$ ($k = 1, 2, \ldots, m$) by fixing one and solving the other as shown in [22] and [32].

Since we are solving for each $\mathbf{w}_k$, by adapting the idea of Sparse Group Lasso [31], the constraints can be replaced by introducing a penalty term or penalty function $h(\cdot)$. In this work, the penalty function $h(\cdot)$ takes the following form

$$h(\mathbf{w}) = (1 - \alpha)||(\mathbf{A}^T(\mathbf{w} \circ \mathbf{w}))^{\circ \frac{1}{2}}||_1 + \alpha ||\mathbf{w}||_1,$$
(15)

where $\alpha \in (0, 1)$ balances the two penalties.

One can show that if the $\mathbf{w}_k$ is known, the solutions of $\boldsymbol{\theta}_k$ of the optimisation problem (13) with the constraints (14) have a closed form solution given by

$$\tilde{\boldsymbol{\theta}}_k = (\mathbf{I}_c - \mathbf{\Theta}_{(k-1)}^T \mathbf{\Theta}_{(k-1)} \mathbf{B}) \mathbf{B}^{-1} \mathbf{Y}^T \mathbf{X} \mathbf{w}_k$$
$$\boldsymbol{\theta}_k = \tilde{\boldsymbol{\theta}}_k / \sqrt{\tilde{\boldsymbol{\theta}}_k^T \mathbf{B} \tilde{\boldsymbol{\theta}}_k},$$
(16)

where $\mathbf{\Theta}_{(k-1)}$ denotes the first $k-1$ columns of $\mathbf{\Theta}$.

In the sequel, the optimisation problem (13, 14) is converted to the following form

$$\min_{\mathbf{w}_k, \boldsymbol{\theta}_k} \frac{1}{2n} || \mathbf{Y}\boldsymbol{\theta}_k - \mathbf{X}\mathbf{w}_k ||_2^2 + \lambda h(\mathbf{w}_k)$$
(17)

$$\text{s.t. } \boldsymbol{\theta}_k^T \mathbf{B} \boldsymbol{\theta}_k = 1$$
$$\boldsymbol{\theta}_k^T \mathbf{B} \boldsymbol{\theta}_i = 0 \quad \forall i < k,$$
(18)

where (18) is converted from the constraint $\mathbf{\Theta}^T \mathbf{B} \mathbf{\Theta} = \mathbf{I}_{m \times m}$ in (14), and $h(\cdot)$ is defined in (15). Such an optimisation problem is convex. This can be solved by applying proximal gradient descent [33].

After obtaining the optimal solution $\mathbf{W}^*$, the features f_i are ranked in descending manner according to the corresponding values of ω_i. Features and sensors ranked highest without violating the constraint on $\boldsymbol{\omega}$ and $\boldsymbol{\psi}$ in (14) are selected. The sensor selection algorithm (*SS-CF*) is summarised in Algorithm 1.

Algorithm 1 *SS-CF* Algorithm

Input : $\mathbf{X} \in \mathbb{R}^{n \times d}$: Training data;
         $\mathbf{Y} \in \mathbb{R}^{n \times c}$: Dummy variable of labels (12);
         $\mathbf{A} \in \mathbb{R}^{d \times p}$: Mapping matrix (4);
         l: Limit in the number of features to utilise;
         q: Limit in the number of sensors to utilise;
         m: Dimension after projection;
         α, λ: Tuning parameters for optimisation;
Output: $\mathbf{W}^* = \left[\mathbf{w}_1^*, \ldots, \mathbf{w}_m^* \right]$: Optimal projection;
         $\mathcal{F}_s$: Selected feature set;
         $\mathcal{G}_s$: Selected sensor set;

1   Initialise: $\mathbf{B} = \frac{1}{n} \mathbf{Y}^T \mathbf{Y}$, $\mathbf{\Theta} = \left[\boldsymbol{\theta}_1, \ldots, \boldsymbol{\theta}_m \right] = \mathbf{I}_{c \times m}$;
2   **for** $k = 1, \ldots, m$ **do**
3   **while** $\mathbf{w}_k$ has not converged **do**
4   Solve for $\mathbf{w}_k$ by solving (17) using proximal gradient descent ;
5   Update $\boldsymbol{\theta}_k$ using (16) ;

6   Rank the features f_i descending based on ω_i^* calculated by (2);
7   Obtain $\mathcal{F}_s$ and $\mathcal{G}_s$ which are the highest ranked sensor and feature indices without violating (14);

III. Human Data Collection and Algorithm Evaluation Experiment

The objective of this study is to develop an algorithm for selecting the sensors that contain the maximum information, thus guaranteeing the highest chance of accurate target pose identification when the user controls the prosthesis in real-time. The implementation of the algorithm for real-time decision-making and joint movement control in a prosthesis will be investigated in our future work. In this section, the proposed *SS-CF* algorithm is validated with the data collected from a human-subject experiment in the context of identifying the target prosthetic pose involving coordinated motion with the upper limb and trunk. The protocol of the human experiment for data collection is presented, followed by the feature extraction methods where the training data $\mathbf{X}$ and $\mathbf{Y}$ are obtained and the mapping matrix $\mathbf{A}$ is constructed. Finally, the experimental protocol for evaluating algorithm performance is presented where l, q, and m are set according to the need, α is chosen as suggested in the literature and λ is optimised by the grid searching method [31].

A. Experimental Protocol for Human Data Collection

1) Subject Recruitment: Ten non-disabled subjects (7 male, 3 female; all right-handed) were recruited for the data collection experiment. The age range was [24, 32] with a
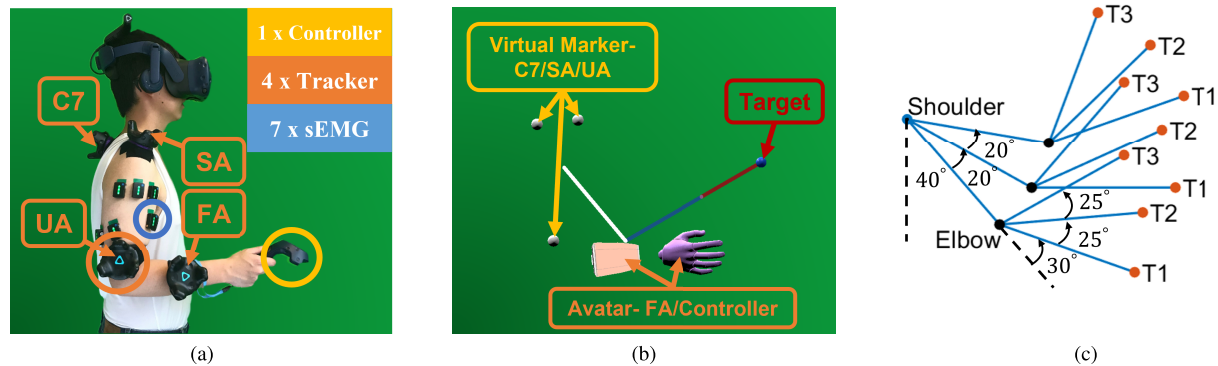
Fig. 1. (a) Experimental setup and sensor deployment, (b) Virtual Reality (VR) avatar and reaching target example, (c) Target set within the parasagittal plane, T1-T3 denote the intended target elbow poses.

median of 27. The experimental protocol was similar to our previous work [29], and described below. It is approved by the University of Melbourne Human Research Ethics Committee, project ID 11878. Informed consents were obtained from all subjects.

2) Experimental Protocol: The experiment was conducted in the context of transhumeral prostheses control where a set of sensors are attached to the upper limb and upper body of the human subjects (Fig. 1(a)) to record the kinematic and sEMG signals. The subjects stand straight naturally and unconstrained, and were asked to perform forward-reaching tasks toward targets placed along the parasagittal plane by extending the upper limb forward, for ten iterations for each target. The target, which the subject should reach with their hand, was displayed in the head-mounted display virtual reality (VR) environment as a sphere, see Fig. 1(b). The position of the target was generated by the subjects flexing the shoulder joint and extending the elbow joint to the designed poses, see Fig. 1(c), and the middle fingertip location in VR environment is recorded as the target location. To instruct the subjects to reach the pose during target generation, the real-time shoulder flexion/extension and elbow flexion/extension poses were displayed in front of the subject's left eye.

The subjects were instructed to maintain their final upper limb pose after reaching the targets. The quasi-static sensor readings during the holding period were used for feature extraction. This data primarily consists of static information about the subject reaching the intended elbow pose and being instructed to hold the pose. Thus, the data is valuable and reliable to detect such intention when the elbow joint has been replaced with a prosthetic component.

3) Task Description: By setting the joint space human arm displacements, nine reaching targets were set in the parasagittal plane as illustrated in Fig. 1(c). The arm-length calibration was resolved by the target generation process.

In the context of a transhumeral prosthesis (for an above-elbow amputation), the prosthesis consists of the elbow (and potentially, the wrist and hand). In this study, only the elbow joint was considered for the prosthesis. In this experiment, the HPI needs to identify the $c = 3$ discrete elbow poses accurately, based on the kinematics (e.g. the shoulder pose)

and the sEMG signals of the human subject. The data set was collected at three distinct shoulder poses and three elbow poses, resulting in the 9 reaching targets in the experiment, labelled as T_i ($i = 1, 2, 3$), as shown in Fig. 1(c).

4) Sensor Deployment: The upper-body and arm kinematic signals and upper-arm sEMG signals were collected using wearable sensors with a sampling rate of 90 Hz and 1,111 Hz, respectively. Fig. 1(a) presents the sensor setup. Upper body and upper arm postural data were acquired through three HTC VIVE Trackers (with motion capture sensors and an embedded IMU) attached to the subject's upper arm (UA), shoulder acromion (SA), and C7 vertebrae (C7). Another tracker on the forearm (FA) and the controller in the hand was only utilised to control the avatar in the VR environment. Seven Delsys® Trigno™ wireless sEMG electrodes were attached to the dominant upper arm of the subjects: two on the biceps long/short heads (BLH/BSH), two on the triceps lateral/long heads (TLAH/TLH), three on the anterior, middle and posterior of the deltoid (DA/DM/DP).

B. Feature Extraction

Based on the type of sensors used, the candidate features were extracted from the data containing the target pose intention. The data were collected during the subject holding the upper-limb pose upon reaching the targets in a coordinated fashion and were summarised in Table III. The training data **X**, dummy variable matrix **Y**, and the mapping matrix **A** are constructed from the feature data.

The time-domain sEMG and joint postural features were utilised in this study. To extract the time-domain sEMG features, the raw sEMG signals were filtered by a 4th order Butterworth band-pass filter with a 10-500 Hz passband [34]. Outliers of more than three standard deviations from the mean were removed. Then, a sliding window of 200ms was applied for the signal, with overlapping 100ms (resulting 10Hz sampling rate). The kinematic postural features were computed through the orientation readings of the embedded IMU of VIVE trackers and were downsampled to 10Hz.

1) Kinematic Postural Features: We included both direct and composite kinematic postural features. The direct features are the trunk flexion/extension (Tf/e) and left/right

TABLE III
COMPOSITE AND DIRECT FEATURES

Modality	Feature Abbrev.	Detail	
		Sensor	Description
Kinematics	Tf/e	C7	Trunk flexion/extension
	Tlb/rb	C7	Trunk left/right bending
	Scp/r*	C7,SA	Scapular protraction/retraction
	Scd/e*	C7,SA	Scapular depression/elevation
	Sf/e*	C7,UA	Shoulder flexion/extension
	Sabd/add*	C7,UA	Shoulder abduction/adduction
sEMG	MAV		Mean absolute value [29]
	WL		Wave length [29]
	RMS	sEMG electrodes: BSH,BLH,TLAH,TLH,DA,DM,DP	Root mean square [29]
	ZC		Zero crossing [29]
	SSC		Slop sign change [29]
	MS*	k-combinations of sEMG electrodes in 5 muscle groups	Muscle synergy (19,20)

* Composite features

bending (Tlb/rb) which only require the C7 tracker's measurements. The composite postural features are: shoulder flexion/extension (Sf/e) and adduction/abduction (Sabd/add) which needs UA and C7 trackers, and scapular protraction/retraction (Scp/r) and depression/elevation (Scd/e) which requires UA and SA trackers. Since the targets were in the parasagittal plane, shoulder internal/external rotation and trunk rotation were not considered.

2) sEMG Features: For sEMG features, the direct and composite features are the time-domain and muscle synergy features, respectively. The time-domain sEMG features are computed following [29], [35], including **mean absolute value** (MAV), **root mean square** (RMS), **wave length** (WL), **zero crossing** (ZC) and **slope sign change** (SSC).

Muscle synergy (MS) features were extracted from the RMS values of a group of sEMG sensors [16]. The Nonnegative Matrix Factorisation (NNMF) is used to extract the features. Assume the d_{rms}−dimensional RMS features from a group of sEMG sensors are sorted into a matrix $\mathbf{X}_{rms} \in \mathbb{R}^{n \times d_{rms}}$ and the muscle synergy features can be obtained by decomposing the $\mathbf{X}_{rms}$ into two nonnegative matrices: (i) $\mathbf{G} \in \mathbb{R}^{d_{rms} \times d_{ms}}$ which is the muscle synergy matrix, (ii) $\mathbf{X}_{ms} \in \mathbb{R}^{n \times d_{ms}}$ which is the muscle synergy features where each column is regarded as a feature. The $d_{ms} < d_{rms}$ is the reduced dimension of the extracted muscle synergies. The relationship is given by

$$\mathbf{X}_{rms}^T = \mathbf{G}\mathbf{X}_{ms}^T + \mathbf{E}, \tag{19}$$

where $\mathbf{E} \in \mathbb{R}^{d_{rms} \times n}$ is the residual which can be used to estimate the variance of the data account explained by the factorisation. In this work, the d_{ms} for each muscle combination was determined based on the criterion: $||\mathbf{E}||_2/||\mathbf{X}_{rms}^T||_2 < 5\%$ which means more than 95% variance of the data is explained by the $\mathbf{G}\mathbf{X}_{ms}^T$. The overall muscle synergy features in this study were from the k-combinations ($k = 2, 3, \ldots, 5$) of five muscle groups (biceps, triceps, deltoid anterior, middle and posterior).

The $\mathbf{G}$ is obtained using the $\mathbf{X}_{rms}$ of the training data. During test The $\mathbf{G}$ is then used to obtain the muscle synergy features $\mathbf{X}_{ms}$ by

$$\mathbf{X}_{ms}^T = \mathbf{G}^\dagger \mathbf{X}_{rms}^T, \tag{20}$$

where $\dagger$ denotes the left Moore–Penrose inverse which satisfies $\mathbf{G}^\dagger = (\mathbf{G}^T\mathbf{G})^{-1}\mathbf{G}^T$.

C. SS-CF Experimental Evaluation

In the evaluation, the proposed *SS-CF* sensor selection algorithm was applied to select q sensors from a total of 10 sensors (where $q = 1$ to 9) that provide the best features to distinguish the target poses, based on the data collected in the aforementioned human subject experiment. The matrix $\mathbf{A}$ is constructed based on the information in Table III. The resultant classification accuracy of the selected features of sensors was used as the performance metric. We conducted 5-fold cross-validation for the dataset from each subject. By doing so, the data are divided into 5 parts each containing 2 iterations, and each part will be reserved for the test with the rest being used for sensor selection and classifier training. Regarding the constraints in (11), we set: $\|\boldsymbol{\psi}\|_0 = q \in [1, 9]$ and $||\boldsymbol{\omega}||_0 \leq l = d$. The upper bound of the number of selected features was set large enough to allow all the informative features to be used. The tuning parameter λ was determined to be the value that results in the closest sensor-level sparsity and minimum cross-validated value of (17) along a grid of λ. The grid was set by log-linearly interpolating 30 points between the $\lambda_{max} = 0.3$ and $\lambda_{min} = 0.1\lambda_{max}$. The adopted parameter settings were: $\lambda_{max} = 0.3$, $\lambda_{min} = 0.03$, $\alpha = 0.95$, $m = 2$. The dimension of the projected feature space m was set such that after the projection, it was possible to view how the classes are separated in the low-dimensional (2D) feature space by observation.

Three sets of performance evaluation, benchmarking and analysis are carried out in this study. They are described below and the results and the corresponding discussions are presented in Section IV (Results and Discussion).

1) Performance Evaluation and Benchmarking: The sensor sets selected by *SS-CF*, for $q = 1$ to 9 were assessed for their classification accuracy using the test data. The performance was also compared to reported sensor selections in the literature, which were carried out based on the experience and knowledge of experts (the experimenters). The two studies in the literature that are used as benchmarks in this paper are:

- [7]: utilises 4 sensors, including C7 and UA trackers to obtain upper limb kinematics and a pair of sEMG electrodes placed at BLH and TLAH;

- [8]: utilises 9 sensors, including all 7 sEMG electrodes in our study and C7 and UA trackers which act similarly to the motion tracking system with bony markers as reported in [8].

Given the studies in the literature were carried out with a specific number of sensors, the comparisons of the outcomes of the proposed algorithm to the literature were only done at $q = 4$ and $q = 9$.

In the evaluation of the classification accuracy of the selected sensors, all the features available to the sensor choices were utilised. The intended pose classification of the sensor sets by *SS-CF* and the two benchmark algorithms from the literature were tested on three classifiers:

- k-**Nearest Neighbors** (KNN) which is a simple nonparametric classifier [36] with nonlinear decision boundaries. The parameter k was tuned through a grid search from 1 to 27 (the square root of the training sample number);
- **Time-delayed Artificial Neural Network** (TDANN) which was used in [8] to predict transhumeral prosthetic poses. The network had a hidden layer with 20 neurons and an input delay of 7 the same as [8];
- **Linear Discriminant Analysis** (LDA) which is a commonly used linear classifier in prostheses control [12].

The statistical significance test was conducted using a non-parametric method because the obtained classification accuracy does not fit the normality assumption [37]. The two-sided Wilcoxon signed-rank test was performed to compare the accuracy between the sensor selection results by our algorithm and the two chosen benchmark selections, at $q = 4$ against [7] and at $q = 9$ against [8]. The confidence level was set to be 95% ($p < 0.05$).

2) Comparison to Greedy Heuristics: Sequential Forward Selection (SFS) is a simple greedy heuristic algorithm that has been used for sensor selection. The algorithm adds one sensor with all available features at a time based on some performance metric (usually classification accuracy) until q sensors are selected [11], [13]. A similar approach can be applied to our problem formulation (10, 11), when l is set sufficiently large. However, the results can be suboptimal [30]. Therefore, we doubt due to the existence of composite features, the optimal sensor set can be non-sequentially built, and the proposed algorithm gives better performance. The classification performance was evaluated using KNN.

3) Inter-Subject Variations: It has been shown that the most informative feature sets vary between subjects in HPIs [11], [29] The proposed algorithm was applied to the data of individual subjects, to select the sensor sets that provide the highest classification accuracy. The selected sensors (at $q = 1$ to 9) based on the first fold of 5-fold cross-validation training data were investigated, and the variations of the selections were compared to get an insight into the inter-subject variations.

IV. Results and Discussion

In this section, the results and discussion for the three points of evaluation outlined in Section III-C are presented.

A. Performance Evaluation and Benchmarking

The performance evaluation of the *SS-CF* algorithm is shown in the three subplots in Fig. 2, for the three classifiers used. The expected general trend was found in the three subplots that as the number of sensors selected gets higher, the accuracy generally increases. Note that there are 10 available sensors to choose from in the training data. It was observed that the *SS-CF* algorithm achieved higher accuracy for all three classifiers when compared to the results of the selection based on expert experience (*4-sensor* [7] and *9-sensor* [8]) with $p < 0.05$. The outcome across three classifiers shows the generalisability of the proposed *SS-CF* algorithm for different machine learning models since it evaluates the statistical properties of the data. Consequently, the sensor selection process can be decoupled from the design and implementation of the machine learning model for HPIs. This can significantly reduce the effort required, such as in [11] and [13], for repetitive training and tuning the hyper-parameters of the HPI model when evaluating each candidate feature and sensor set.

In addition to the systematic nature of the proposed approach, and the potential higher accuracy in identifying the intended target pose, the increase in performance can also allow the same performance to be achieved with fewer sensors, reducing system complexity. Fig. 2 also shows that the accuracy did not increase proportionally to the further increase in the number of sensors.

It is noteworthy that the highest mean classification accuracy shown in Fig. 2(a) was obtained by selecting only two sensors. However, it is observed that the accuracy variance at $q = 2$ is quite large and decreases for larger q. Therefore, we think the peak of the mean accuracy observed at $q = 2$ is a consequence of the large inter-subject variation and is not representative of the overall performance of all 10 subjects at $q = 2$. This is further supported by the observations in Fig. 3 which shows the performance of two subjects, S8 (Fig. 3(a)) and S10 (Fig. 3(b)). It is observed that the accuracy of the two subjects has a significant difference at $q = 2$, with each deviating significantly from the mean accuracy in opposite directions. The achieved accuracy for S8 is much higher than S10 (100 % vs. 85%). This figure also shows that the variation in the accuracy decreases at larger q values. Furthermore, this result shows that personalisation of the HPI is required when a low number of sensors are used [11], [29].

B. Comparison to Greedy Heuristics

A comparison is made between the outcome of the proposed *SS-CF* algorithm and a sequential forward selection (SFS) process. The outcome presented in Fig. 3 indicates that the optimal sensor set may be non-sequentially built to the ascending number of sensors. The SFS approach selects the best sensor when only $q = 1$ sensor can be selected. Then for the case of selecting $q = 2$ sensors, it assumes the sensor that is best for the scenario of $q = 1$ is included and searches for a second sensor to complete the set of 2 sensors, and so on. Fig. 3 demonstrates the sensors selected for $q = 1$ to 9 for 2 different subjects (subject 8 (S8) and subject 10 (S10), shown in Fig. 3(a) and 3(b), respectively). For Fig. 3(a), it was
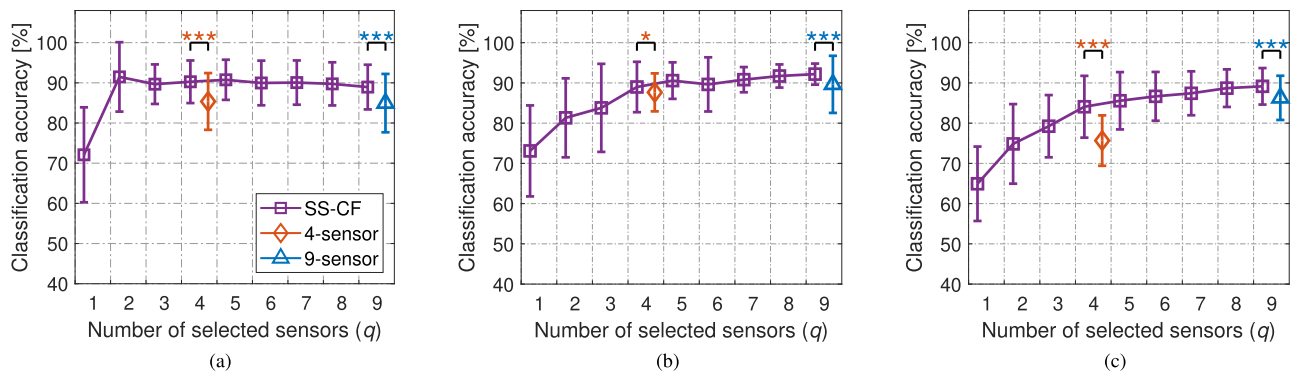
Fig. 2.   The resultant classification accuracy of 3 elbow poses using the selected sensor and feature sets by the proposed *SS-CF* algorithm and compared to 2 existing results with *4-sensor* [7] and *9-sensor* [8]: (a) *k*-Nearest Neighbors (KNN) classifiers, (b) Time-delayed artificial neural network (TDANN) and (c) Linear Discriminant Analysis (LDA). The error bars represent the population mean accuracies and their standard deviation. The statistical significance test results are shown at the top with * denoting $p < 0.05$, ** denoting $p < 0.01$, and *** denoting $p < 0.001$.
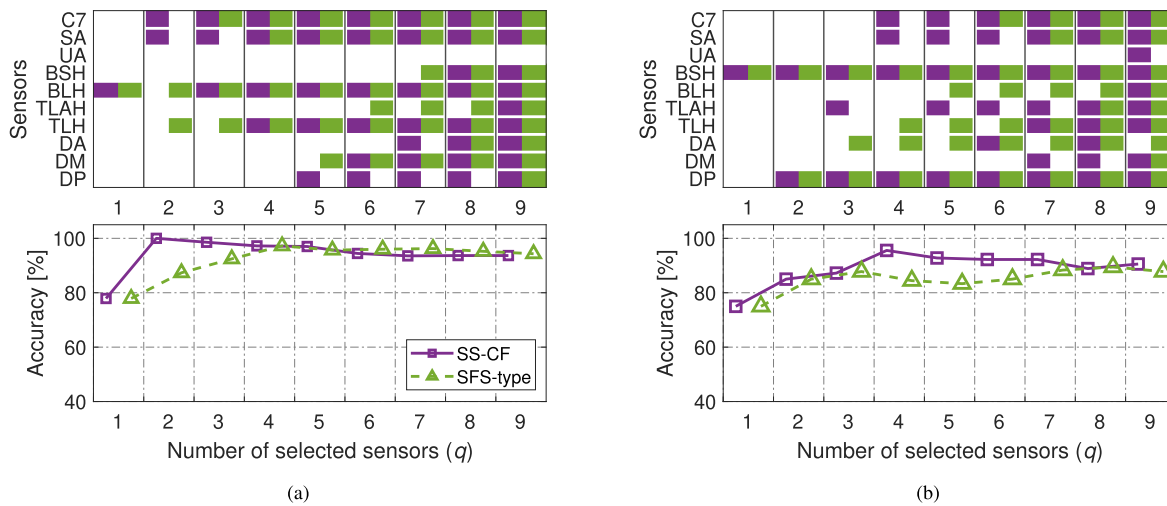
Fig. 3.   (a) and (b) demonstrate the comparison of the proposed *SS-CF* vs. Sequential-Forward-Selection (SFS) type solution to the proposed problem formulation for two of the subjects, S8 and S10, respectively. The top row shows the sensor selection results where the colored block indicates the chosen sensor. For each q, the selections by the proposed method are on the left (in purple), and the SFS-type results are on the right (in green), respectively. The bottom row shows the corresponding elbow pose classification accuracy using KNN classifier by the chosen sensors and features based on the two methods.

shown that for this subject, for $q = 2$, the outcome of the convex-relaxation-based *SS-CF* algorithm does not contain the sensor selected for $q = 1$. Similarly, for Fig. 3(b) at $q = 4$. In both cases, the classification performance is significantly better than the SFS-type solution (the bottom row).

To be specific, for subject 8 (S8), BLH is the best single sensor, whereas C7 and SA form the sensor pair which can provide the composite feature Scp/r and Scd/e and performs significantly better. This is mainly due to the composite features, building up the sensor set sequentially is very likely to miss such features in other possible sensor combinations. The proposed *SS-CF* algorithm results in the selection of the C7 and SA kinematic sensors, while the SFS-type algorithm fails to include these sensors at $q = 2$, leading to suboptimal results. Similarly, the suboptimal path starts from $q = 4$ for subject 10 (S10).

C. Inter-Subject Variations

The variation in the resulting sensor selection among different subjects was investigated. As shown in Fig. 3,

different sensor sets are selected for the subjects S8 and S10, for $q = 1, \ldots, 9$ sensor sets. Fig. 4 further presents such variation among the 10 subjects, by depicting the occurrence percentage of each sensor being selected among the 10 subjects for $q = 1, \ldots, 9$. For example, for $q = 1$, sensor C7 was selected for two of the 10 subjects. None of the q sensors result in the same sets among the 10 subjects. In other words, for any q, there are no q sensors selected for all subjects. For $q = 1$ and 2, there was not one single sensor that was selected for all subjects. The most commonly selected was BLH at $q = 1$ and C7 and SA at $q = 2$. Even at $q = 9$, only 7 sensors are common among all subjects (selected for 100% of the subjects). Consequently, the results in this subsection and IV-A indicated that personalisation in feature selection [28], [29] and sensor selection yield significant performance improvements.

D. Limitations and Future Work

Although the classification accuracy is a reasonable metric herein for evaluating the selected sensor's information in
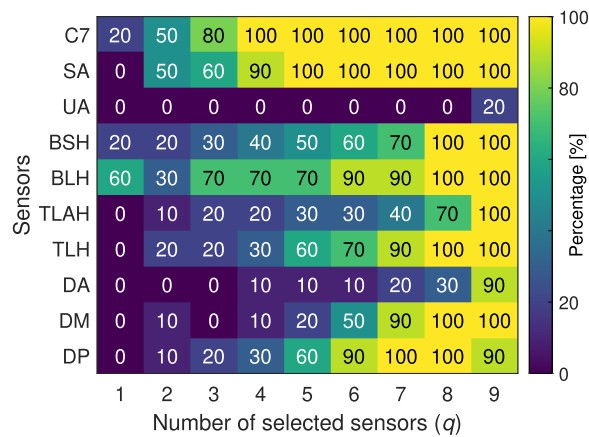
Fig. 4. The occurrence percentage of each sensor being selected for $q = 1, 2, \ldots, 9$ sensors among the 10 subjects. The lighter the color, the higher occurrence of the sensor selected.

differentiating the user intention. This metric may not fully reflect the performance when the human user controls the prosthesis in real time since the transient data during dynamic movement can be substantially different. Frequent misclassification of the target prosthetic poses might happen and hinder the subjects to reach the intended upper-limb pose efficiently in an online manner. However, the online performance of prosthesis control depends predominately on the implementation of control algorithms, including the method for making decisions, joint motion planning, and control. Therefore, the next key problem would be how to process data when the user is in the loop.

The target pose set in this work was limited to three poses of one prosthetic elbow joint. The targets lie only in the parasagittal plane and are non-oriented. From the perspective of benefiting the advance in the multi-DoF prosthesis, it is necessary to extend the workspace from a plane to the 3-dimensional physical space and densify it in terms of the pose resolution of multiple DoFs. To this end, a corresponding extended and densified target pose set can be constructed for data collection. Then, the proposed algorithm can be applied to each DoF, selecting sensors and evaluating offline performance. If low performance is observed, we can use the "class separability" measure $tr(\mathbf{S}_w^{-1}\mathbf{S}_b)$ to identify challenging poses with a low separability. To address this, we may explore other input modalities or include a user training stage [38].

In addition to selecting individual sensors, our proposed algorithm can be used to systematically screen sensor modalities. For example, in detecting human intention for assistive devices, various modalities can be used, such as EMG, kinematics, electroencephalogram (EEG), force myography (FMG), gaze tracking sensors, etc. In order to apply our algorithm, each modality can be treated as a "sensor", and the $\mathbf{A}'$ matrix can be constructed accordingly. The $\mathbf{A}'$ matrix enables the identification of composite features that require information from multiple modalities. The proposed algorithm is applicable to other applications in the presence of composite features beyond the one studied in this article. For instance, it can also be applied to select

sensors for predicting the user intention in assistive lower limb exoskeletons [39], [40]. Furthermore, our proposed problem formulation can be applied in cases where ground truth labels are not available, such as in the detection of back injury risk in [41], or in unsupervised scenarios like the Body-Machine Interface studied in [42].

V. CONCLUSION

In this paper, a sensor selection problem in the presence of *composite* features is formulated and solved specifically for an HPI application. The proposed *SS-CF* optimisation-based approach was found to outperform the benchmark sensor selection results reported in the literature for the same number of sensors utilised. Compared to the heuristic approach of sequential forward selection (SFS), the proposed convex-relaxation based optimisation approach was found to provide higher accuracy in identifying the intended target poses. This is because the SFS approach adds one sensor at a time to the set of candidate sensors, which does not take into account the composite features that require inputs from specific multiple sensors. Evaluating the resulting selected sensors for different individuals demonstrated a high degree of inter-subject variations, which supports the cause for personalisation of HPIs.

ACKNOWLEDGMENT

REFERENCES

[1] R. Garcia-Rosas, D. Oetomo, C. Manzie, Y. Tan, and P. Choong, "Task-space synergies for reaching using upper-limb prostheses," *IEEE Trans. Neural Syst. Rehabil. Eng.*, vol. 28, no. 12, pp. 2966–2977, Dec. 2020.

[2] R. Garcia-Rosas, Y. Tan, D. Oetomo, C. Manzie, and P. Choong, "Personalized online adaptation of kinematic synergies for human-prosthesis interfaces," *IEEE Trans. Cybern.*, vol. 51, no. 2, pp. 1070–1084, Feb. 2021.

[3] S. Mick et al., "Shoulder kinematics plus contextual target information enable control of multiple distal joints of a simulated prosthetic arm and hand," *J. NeuroEngineering Rehabil.*, vol. 18, no. 1, pp. 1–17, Dec. 2021.

[4] R. Garcia-Rosas, T. Yu, D. Oetomo, C. Manzie, Y. Tan, and P. Choong, "Exploiting inherent human motor behaviour in the online personalisation of human-prosthetic interfaces," *IEEE Robot. Autom. Lett.*, vol. 6, no. 2, pp. 1973–1980, Apr. 2021.

[5] C. P. Swami, N. Lenhard, and J. Kang, "A novel framework for designing a multi-DoF prosthetic wrist control using machine learning," *Sci. Rep.*, vol. 11, no. 1, pp. 1–13, Jul. 2021.

[6] M. Merad et al., "Assessment of an automatic prosthetic elbow control strategy using residual limb motion for transhumeral amputated individuals with socket or osseointegrated prostheses," *IEEE Trans. Med. Robot. Bionics*, vol. 2, no. 1, pp. 38–49, Feb. 2020.

[7] N. A. Alshammary, D. A. Bennett, and M. Goldfarb, "Synergistic elbow control for a myoelectric transhumeral prosthesis," *IEEE Trans. Neural Syst. Rehabil. Eng.*, vol. 26, no. 2, pp. 468–476, Feb. 2018.

[8] A. Akhtar, N. Aghasadeghi, L. Hargrove, and T. Bretl, "Estimation of distal arm joint angles from EMG and shoulder orientation for transhumeral prostheses," *J. Electromyogr. Kinesiol.*, vol. 35, pp. 86–94, Aug. 2017.

[9] D. Blana, T. Kyriacou, J. M. Lambrecht, and E. K. Chadwick, "Feasibility of using combined EMG and kinematic signals for prosthesis control: A simulation study using a virtual reality environment," *J. Electromyography Kinesiol.*, vol. 29, pp. 21–27, Aug. 2016.

[10] M. Legrand et al., "Simultaneous control of 2DOF upper-limb prosthesis with body compensations-based control: A multiple cases study," *IEEE Trans. Neural Syst. Rehabil. Eng.*, vol. 30, pp. 1745–1754, 2022.

[11] A. Krasoulis, S. Vijayakumar, and K. Nazarpour, "Multi-grip classification-based prosthesis control with two EMG-IMU sensors," *IEEE Trans. Neural Syst. Rehabil. Eng.*, vol. 28, no. 2, pp. 508–518, Feb. 2020.

[12] L. J. Hargrove, E. J. Scheme, K. B. Englehart, and B. S. Hudgins, "Multiple binary classifications via linear discriminant analysis for improved controllability of a powered prosthesis," *IEEE Trans. Neural Syst. Rehabil. Eng.*, vol. 18, no. 1, pp. 49–57, Feb. 2010.

[13] H.-J. Hwang, J. Mathias Hahne, and K.-R. Müller, "Channel selection for simultaneous and proportional myoelectric prosthesis control of multiple degrees-of-freedom," *J. Neural Eng.*, vol. 11, no. 5, Oct. 2014, Art. no. 056008.

[14] G. R. Naik, A. H. Al-Timemy, and H. T. Nguyen, "Transradial amputee gesture classification using an optimal number of sEMG sensors: An approach using ICA clustering," *IEEE Trans. Neural Syst. Rehabil. Eng.*, vol. 24, no. 8, pp. 837–846, Aug. 2016.

[15] G. Averta et al., "On the time-invariance properties of upper limb synergies," *IEEE Trans. Neural Syst. Rehabil. Eng.*, vol. 27, no. 7, pp. 1397–1406, Jul. 2019.

[16] C. W. Antuvan, F. Bisio, F. Marini, S.-C. Yen, E. Cambria, and L. Masia, "Role of muscle synergies in real-time classification of upper limb motions using extreme learning machines," *J. NeuroEngineering Rehabil.*, vol. 13, no. 1, pp. 1–15, Dec. 2016.

[17] M. Legrand, M. Merad, E. de Montalivet, A. Roby-Brami, and N. Jarrassé, "Movement-based control for upper-limb prosthetics: Is the regression technique the key to a robust and accurate control?" *Frontiers Neurorobotics*, vol. 12, pp. 1–13, Jul. 2018.

[18] M. Legrand, N. Jarrasse, E. D. Montalivet, F. Richer, and G. Morel, "Closing the loop between body compensations and upper limb prosthetic movements: A feasibility study," *IEEE Trans. Med. Robot. Bionics*, vol. 3, no. 1, pp. 230–240, Feb. 2021.

[19] J.-J. Wang, F. Xue, and H. Li, "Simultaneous channel and feature selection of fused EEG features based on sparse group lasso," *BioMed Res. Int.*, vol. 2015, pp. 1–13, Feb. 2015.

[20] L. Pelaez Murciego, M. C. Henrich, E. G. Spaich, and S. Dosen, "Reducing the number of EMG electrodes during online hand gesture classification with changing wrist positions," *J. NeuroEngineering Rehabil.*, vol. 19, no. 1, pp. 1–16, Dec. 2022.

[21] C. L. Pulliam, J. M. Lambrecht, and R. F. Kirsch, "EMG-based neural network control of transhumeral prostheses," *J. Rehabil. Res. Dev.*, vol. 48, no. 6, pp. 739–754, 2011.

[22] L. Clemmensen, T. Hastie, D. Witten, and B. Ersbøll, "Sparse discriminant analysis," *Technometrics*, vol. 53, no. 4, pp. 406–413, Jan. 2011.

[23] T. Hastie, A. Buja, and R. Tibshirani, "Penalized discriminant analysis," *Ann. Statist.*, vol. 23, no. 1, pp. 73–102, 1995.

[24] J. Gui, Z. Sun, S. Ji, D. Tao, and T. Tan, "Feature selection based on structured sparsity: A comprehensive study," *IEEE Trans. Neural Netw. Learn. Syst.*, vol. 28, no. 7, pp. 1490–1507, Jul. 2017.

[25] F. Nie, Z. Wang, L. Tian, R. Wang, and X. Li, "Subspace sparse discriminative feature selection," *IEEE Trans. Cybern.*, vol. 52, no. 6, pp. 4221–4233, Jun. 2020.

[26] T. Pang, F. Nie, J. Han, and X. Li, "Efficient feature selection via $\ell_{2,0}$-norm constrained sparse regression," *IEEE Trans. Knowl. Data Eng.*, vol. 31, no. 5, pp. 880–893, May 2019.

[27] R. Reams, "Hadamard inverses, square roots and products of almost semidefinite matrices," *Linear Algebra Appl.*, vol. 288, pp. 35–43, Feb. 1999.

[28] T. Yu, R. Garcia-Rosas, A. Mohammadi, Y. Tan, P. Choong, and D. Oetomo, "Separability of input features and the resulting accuracy in classifying target poses for active transhumeral prosthetic interfaces," in *Proc. 43rd Annu. Int. Conf. IEEE Eng. Med. Biol. Soc. (EMBC)*, Nov. 2021, pp. 4615–4618.

[29] T. Yu, R. Garcia-Rosas, A. Mohammadi, Y. Tan, P. Choong, and D. Oetomo, "Comparing the outcomes of population-averaged and personalised input feature selection for transhumeral prosthetic interfaces," in *Proc. IEEE Int. Conf. Syst., Man, Cybern. (SMC)*, Oct. 2021, pp. 417–422.

[30] K. Fukunaga, *Introduction to Statistical Pattern Recognition* (Computer Science and Scientific Computing). New York, NY, USA: Academic, 1990.

[31] S. Noah, J. Friedman, T. Hastie, and R. Tibshirani, "A sparse-group lasso," *J. Comput. Graph. Stat.*, vol. 22, no. 2, pp. 231–245, 2013.

[32] K. Sjöstrand, L. H. Clemmensen, R. Larsen, G. Einarsson, and B. Ersbøll, "SpaSM: A MATLAB toolbox for sparse statistical modeling," *J. Stat. Softw.*, vol. 84, no. 10, pp. 1–37, 2018.

[33] J. Klosa, N. Simon, P. O. Westermark, V. Liebscher, and D. Wittenburg, "Seagull: Lasso, group lasso and sparse-group lasso regularization for linear regression models via proximal gradient descent," *BMC Bioinf.*, vol. 21, no. 1, pp. 1–8, Dec. 2020.

[34] A. Stango, F. Negro, and D. Farina, "Spatial correlation of high density EMG signals provides features robust to electrode number and shift in pattern recognition for myocontrol," *IEEE Trans. Neural Syst. Rehabil. Eng.*, vol. 23, no. 2, pp. 189–198, Mar. 2015.

[35] A. Phinyomark, P. Phukpattaranont, and C. Limsakul, "Feature reduction and selection for EMG signal classification," *Exp. Syst. Appl.*, vol. 39, pp. 7420–7431, Jun. 2012.

[36] M. Zardoshti-Kermani, B. C. Wheeler, K. Badie, and R. M. Hashemi, "EMG feature evaluation for movement control of upper extremity prostheses," *IEEE Trans. Rehabil. Eng.*, vol. 3, no. 4, pp. 324–333, Dec. 1995.

[37] J. Demšar, "Statistical comparisons of classifiers over multiple data sets," *J. Mach. Learn. Res.*, vol. 7, pp. 1–30, Jan. 2006.

[38] J. L. Nawfel, K. B. Englehart, and E. J. Scheme, "The influence of training with visual biofeedback on the predictability of myoelectric control usability," *IEEE Trans. Neural Syst. Rehabil. Eng.*, vol. 30, pp. 878–892, 2022.

[39] G. Yin et al., "Processing surface EMG signals for exoskeleton motion control," *Frontiers Neurorobotics*, vol. 14, p. 40, Jul. 2020.

[40] J. Fong, K. Bernacki, D. Pham, R. Shah, Y. Tan, and D. Oetomo, "Exploring the utility of crutch force sensors to predict user intent in assistive lower limb exoskeletons," in *Proc. Int. Conf. Rehabil. Robot. (ICORR)*, Jul. 2022, pp. 1–6.

[41] M. Robinson, L. Lu, Y. Tan, D. Oetomo, and C. Manzie, "Feature identification framework for back injury risk in repetitive work with application in sheep shearing," *IEEE Trans. Biomed. Eng.*, vol. 70, no. 2, pp. 616–627, Feb. 2023.

[42] F. Rizzoglio, M. Giordano, F. A. Mussa-Ivaldi, and M. Casadio, "A non-linear body machine interface for controlling assistive robotic arms," *IEEE Trans. Biomed. Eng.*, early access, Jan. 16, 2023, doi: 10.1109/TBME.2023.3237081.